Cryogenic Ion Vibrational Spectroscopy of

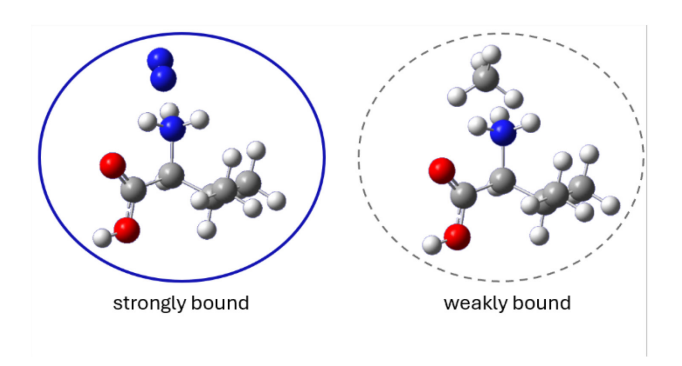
Protonated Valine: Messenger Tag Effects

Lane M. Terry, Maddie K. Klumb, Deacon J. Nemchick, Robert Hodyss, Frank Maiwald, and J. Mathias Weber^{1,*}

¹ JILA and Department of Chemistry, University of Colorado Boulder, 440 UCB, Boulder, CO 80309-0440, USA

² NASA Jet Propulsion Laboratory, California Institute of Technology, Pasadena, CA 91109, USA

TOC Graphic



Abstract

We report the infrared photodissociation spectrum of tagged protonated valine in the range of 1000 – 1900 cm⁻¹, prepared in a cryogenic ion trap. Comparison of experimental results with calculated infrared spectra based on density functional theory shows that the hydroxyl group of the carboxylic acid functionality and the protonated amine group adopt a *trans* configuration. Nitrogen and methane molecules were used as messenger tags, with optimal tagging temperatures of 30 K for N₂ and 60 K for CH₄. While the calculated infrared spectra of the tagged ion suggest only a weak influence of the messenger tag on the frequency positions of ValH⁺, the measured intensities for N₂-tagged ValH⁺ appear strongly suppressed for all but the highest frequency feature at 1773 cm⁻¹. We trace this behavior to the binding energy of the N₂ tag, which is significantly higher than that of CH₄, based on density functional and coupled cluster calculations and rate estimates for photoinduced unimolecular dissociation from statistical theory.

Introduction

The search for chemical markers of life or of prebiotic conditions supporting the development of life is at the forefront of astrobiology. Radio astronomy and infrared (IR) spectroscopy have led to the discovery of numerous molecular species¹ in the interstellar medium, as well as in the outflow of carbon rich stars, and much hope rests on future detection of biomarkers by the James Webb Space Telescope.² Closer to home, one of the most promising avenues for the detection and analysis of complex molecules that can serve as biomarkers is through planetary probes on worlds in our own solar system. Using terrestrial biology as a starting point, suitable biomarkers include simple amino acids, nucleobases, sugars, or fatty acids, and candidate worlds range from planets like Mars to planetary moons and planetoids, especially icy worlds with a subsurface aqueous ocean such as Titan, Enceladus, or Europa.

Mass spectrometry provides a powerful approach for the detection of polyatomic molecules, and it has been or will be used on several planetary missions,³⁻⁵ e.g., on the Viking lander (Mars), Curiosity rover (Mars), Rosetta/Philae Lander (Churyumov-Gerasimenko comet), and the planned Rosalind Franklin rover (Mars), and Dragonfly rotorcraft (Titan). However, while mass spectrometers with sufficient resolution can distinguish between ions with very similar masses, e.g., N₂+ (28.0134 u) and CO+ (28.0101 u), mass spectrometry alone is insufficient to identify a molecular ion that could have different structures with the same atomic composition. Using valine (Val, C₅H₁₁NO₂) as an example, the NIST chemistry webbook⁶ identifies more than 30 unique compounds with the same atomic composition, but distinct structure, out of which only valine is a proteinogenic amino acid. Consequently, additional information is required for the unambiguous identification of more complex molecular biomarkers, such as amino acids. Fragmentation patterns from collision induced dissociation experiments can narrow down the candidates for a given

molecular ion, which have very different functional groups (e.g., amino acids and nitrites), but such fragmentation patterns depend significantly on the experimental details. Alternatively, instrumentation operating in concert with mass spectrometry may offer additional information. For example, ion mobility front ends can bring additional structural information. However, ion mobility ultimately only yields a single data point, namely the orientation-averaged collision cross section of the ion in question, and ion mobility collision cross sections may be ambiguous.⁷ Chromatography front ends are complex, and standardization of elution presents significant engineering challenges. Additional channels of information are desirable to unambiguously identify the molecular structure of ions detected in mass spectrometry instruments on planetary missions.

Infrared spectroscopy of mass selected ions in concert with quantum chemical calculations has been shown to be a valuable tool to determine the molecular structure of ions in vacuo, and it has been used extensively in the study of biomolecules. With its power to encode molecular structure, IR spectroscopy can offer an approach towards unambiguous identification of complex molecular ions, including isomers of protonated amino acids such as valine with similar functional groups (see Supporting Information, Figure S1). Libraries of laboratory spectra are needed to make such identifications possible for a large variety of possible biomarkers. While the spectra of several protonated 12-14, 16-19, 21, 24 and deprotonated 23 amino acids have been measured at room temperature using IR multiphoton dissociation (IRMPD), much fewer IR spectroscopy data exist on cryogenically prepared amino acid ions 15, 28, 29 outside of studies on peptides containing several amino acid residues.

Cryogenic ion vibrational spectroscopy (CIVS) allows the use of single photon predissociation by employing weakly bound messenger tags (e.g., H₂, D₂, N₂), yielding IR

photodissociation spectra that correspond closely to the absorption spectra of the target ions, typically with linewidths that are narrow compared to many IRMPD signatures at room temperature and with only small tag-induced shifts. The technique is in principle compatible with trap-based mass spectrometry technology employed on planetary probes. However, the usable temperature range for a given messenger tag is typically relatively narrow, (e.g., 10-15 K for D₂, 25-40 K for N₂), and the tagging temperatures are often significantly lower than the temperatures of target worlds on which CIVS might be employed (e.g., 46 - 96 K on Europa; 30 33 – 145 K on Enceladus;³¹ 110 – 235 K on Ceres;³² 95 K on Titan³³). Active cooling would introduce additional electrical power requirements as well as weight, which is difficult within the typical limitations on both resources on planetary probes. For the prospect of using CIVS on such missions it is therefore desirable to find suitable alternative tags which can function at higher temperatures. We note that tag-free spectroscopy methods may be explored for this purpose, notably IRMPD, laser-induced reactions, or tagging inhibition. However, the laser power requirements of IRMPD are currently prohibitive for laser sources that would fit into missions with limits on weight and electrical power typical for planetary probes. Vibration-induced ion reactions³⁴ likely lack the chemical generality of CIVS. Laser-induced inhibition of complex formation³⁵ is based on depletion signals, which makes this approach less sensitive than CIVS, which is an action technique. Methods exploiting vibration-translation energy transfer³⁶ may be useful, but have not yet been used in the mass range relevant for biomarkers.

In this work, we use CIVS to measure the IR fingerprint spectra of protonated Val (ValH⁺), supported by density functional theory (DFT). We provide an experimental case study on distinguishing different constitutional isomers, comparing the experimental spectrum of ValH⁺,

with DFT calculated spectra of potential isomers. We compare messenger tagging of ValH⁺ with N₂ and CH₄, both in terms of optimal tagging temperatures and photodissociation efficiency.

Methods

The experimental setup has been described in earlier work.³⁷ Briefly, we prepared protonated molecular species by electrospray ionization (ESI) of a 1 mM solution of L-Val (Sigma-Aldrich) in 2:1 acetonitrile (ACN, Thermo Fisher Scientific) and water, with drops of hydrochloric acid (HCl, Mallinckrodt Chemicals) added until the solution was at a pH of 2. Ions passed through a heated desolvation capillary (80 °C) and a skimmer into a series of octopole ion guides and ion optics, which transferred the ions into a Paul trap mounted on a closed cycle He cryostat. In the trap, the ions were accumulated, cooled, and tagged with a single N₂ tag or a single CH₄ tag. The buffer gas in the trap is used for translational and – more importantly – vibrational cooling of the stored ions. Similar to others in the field, 28, 29 we have found light buffer gases containing molecular species optimal for this process. For methane tagging, neat CH₄ was pulsed into the trap and used as the buffer gas, and the optimal trap temperature for tagging was ca. 60 K. The resulting pressure of CH₄ in the trap can be estimated as ca. 2·10⁻³ mbar. For N₂ tagging, we used residual N₂ from the ESI source inlet, together with pulsed injection of 10% D₂ in He as the buffer gas in the trap, and the trap was held at ca. 30 K. As a result, the partial pressure of N₂ in the trap is more difficult to quantify, although the overall pressure in the trap is of the same order of magnitude as for methane buffer gas. The temperatures reported here are the average of two temperature probes, one at the top of the trap near the cold head and one at the bottom of the trap. The difference between the two probes is 12-15 K.

The contents of the ion trap were injected into the acceleration region of a time-of-flight mass spectrometer, and target ions $ValH^+$ tag were subsequently mass-selected in the first space focus using an interleaving comb mass gate and irradiated with the output of a tunable OPO/OPA (LaserVision, pulse duration 5-7 ns, pulse energy ≤ 1.0 mJ). Photofragments of $ValH^+$ following the reaction

$$ValH^+ \cdot tag + \hbar\omega_{IR} \rightarrow ValH^+ + tag$$

were separated from undissociated parent ions in a two-stage reflectron, and the photofragment ion intensity was monitored on a microchannel plate detector as a function of IR wavelength. Ion signals from sixteen shots were averaged for each wavelength in each scan. Background signals from unimolecular dissociation caused by collisional activation during ion ejection from the trap were negligible for ions tagged with N_2 , which allowed us to use a longer cooling and tagging time (100 ms). For CH₄ tagging, only every other ion package was irradiated, and the signals with and without irradiation were subtracted. Keeping the laser repetition rate at 10 Hz, this required running the trap and mass spectrometer at 20 Hz, limiting the cooling and tagging interval to 50 ms. Multiple spectra taken over several days were averaged for each species to improve the signal-to-noise ratio and to ensure reproducibility. Spectra were taken in the fingerprint region (1000 – 1900 cm⁻¹) and calibrated to the known spectrum of acetone³⁸ using a photoacoustic cell, and we assume the calibration to be accurate to within 3 cm⁻¹. We note that photodissociation signals were low for ValH⁺· N_2 , resulting in a relatively low signal-to-noise ratio, despite the fact that the spectra we report represent the average of at least 50 scans.

Structures of the species under study were calculated using DFT,³⁹ geometry optimization runs beginning with several starting structures for each ion. We employed the B3LYP functional⁴⁰, ⁴¹ and cc-pVTZ basis sets^{42, 43} for all atoms. For each minimum energy structure of ValH⁺, the IR

spectrum was calculated based on the harmonic approximation, scaling the frequencies by 0.9889, using a comparison of calculated and experimental data found for the antisymmetric OCO stretching vibration of the carboxylic acid group of protonated alanine.²⁹ In all calculated spectra, vibrational lines are shown as Lorentzians with 8 cm⁻¹ full width at half-maximum.

Binding energies of the tags were calculated with the same method as the geometry optimization, applying the counterpoise method^{44, 45} to correct basis set superposition errors. In addition, we used the optimized geometries from the DFT calculations to determine binding energies at the CCSD⁴⁶ and CCSD(T)^{47, 48} levels of theory with cc-pVDZ and cc-pVTZ basis sets^{42, 43} for the former and cc-pVDZ for the latter. All calculations were performed using the Gaussian 16 program suite.⁴⁹

Results and Discussion

The formation of tagged ions is the result of three-body collisions between the ion, the neutral tag, and a third collision partner. The dependence of this process on temperature is complicated, since the temperature impacts both the available tag density (through its vapor pressure) and the three-body collision cross section. As a practical consideration, in order to form a complex of a neutral messenger tag and ValH⁺, the trap temperature must be chosen to create optimal conditions regarding the vapor pressure and binding energy of the tag. If the trap is too warm, the complex will have sufficient internal energy to induce loss of the tag. If the trap is too cold, the gaseous tag will have insufficient vapor pressure to efficiently form the desired complex. Figure 1 shows the abundance of ion-tag complexes as a function of temperature for both N₂ and CH₄ tags. The temperature range for tagging of ValH⁺ with N₂ is 20-65 K with an optimum at ca. 30 K. For CH₄ tags the optimal temperature range is 50-75 K with an optimum at ca. 60 K.

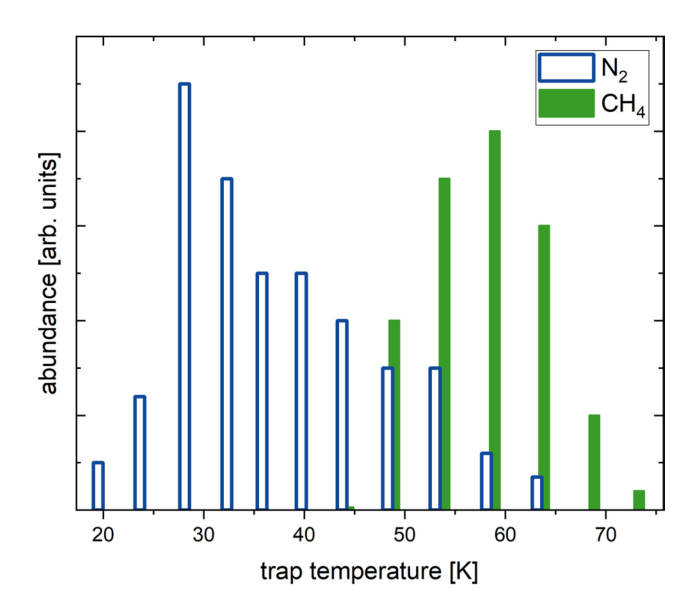


Figure 1. Abundance of ValH⁺ tagged with N_2 (blue, open bars) and with CH₄ (green, full bars) as a function of trap temperature. The peak tagging efficiency (i.e., the fraction of tagged ValH⁺ compared to bare ValH⁺) for each gas is $\leq 5\%$ under the conditions used here, and the scaling of the two data sets is the same.

Protonated valine, ValH⁺, has several possible conformations, which can be roughly classified by the position of the protonated amine group relative (*cis* or *trans*) to the OH group of the COOH carboxylic acid moiety (Figure 2). As one would expect, the lowest energy structure has a *trans* configuration (*trans*-1), which is stabilized by intramolecular hydrogen bonding (H-bonding) to the carboxylic acid group. This structure is significantly lower in energy (by 191 meV) than the lowest energy *cis* (*cis*-1) configuration, which lacks this stabilization. There are overall three low-lying *trans* configurations of ValH⁺ (*trans*-2 at 56 meV and *trans*-3 at 70 meV higher than *trans*-1), which have different orientations of the two methyl groups relative to the NH₃⁺ and COOH groups. We note that similar low-lying conformers were found in earlier computational work by Quesada-Moreno et al.⁵⁰ The geometries discussed there were calculated for different protonation

states of valine embedded in a polarizable continuum, which explains the differences compared to the gas phase structures in the present work.

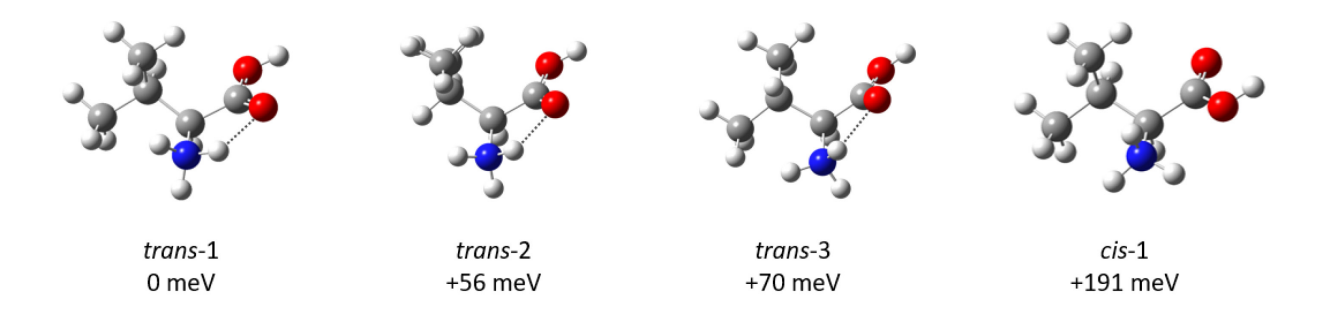


Figure 2. Lowest energy structures of protonated L-Val (ValH $^+$), with three *trans* and one *cis* configuration. The zero-point corrected relative energies are given for each structure. C = grey, H = white, N = blue, O = red. Hydrogen bonds are shown as dotted lines.

The IR photodissociation spectra of ValH⁺·N₂ and ValH⁺·CH₄ are shown in Figure 3, together with the calculated IR spectra of the lowest energy *trans* and *cis* structures of ValH⁺. Consistent with the energetic ordering, the experimental spectrum is more consistent with the calculated spectra for a *trans* configuration than with a *cis* structure. Based on the calculated spectrum of the lowest energy isomer (*trans*-1), we assign the most intense transition (labeled a in Figure 3) around 1775 cm⁻¹ to the antisymmetric OCO stretching vibration of the carboxylic acid group, which is coupled to an HNC bending motion of the H-bonded NH group. A weak, broad peak around 1585 cm⁻¹ (b) can be assigned to two NH₃⁺ scissoring modes. Another weak peak at 1478 cm⁻¹ (c) contains several unresolved transitions characterized by CH₃ scissoring modes. The prominent feature at ca. 1444 cm⁻¹ (d) is mostly due to the NH₃⁺ umbrella motion. This pattern of motion also contributes to the peak at ca. 1415 cm⁻¹ (e) which is mainly carried by a HOC bending and symmetric OCO stretching motion of the COOH group. We assign the weak feature at 1355 cm⁻¹

(f) to a CCH bending motion of the two CH groups attached to the carbon atoms of the central C–C bond. The peak at ca. 1170 cm⁻¹ (g) belongs to a mode mainly due to OH bending motion, while the peak around 1125 cm⁻¹ (h) comes from two modes displaying CH₃/NH₃⁺ tilting motions, and feature (i) at ca. 1080 cm⁻¹ can be traced to similar motions. The simulated spectra of the different *trans* isomers show subtle differences (see Supporting Information, Figure S2), and most key features are sufficiently similar that it is challenging to distinguish between them spectroscopically. However, the signatures between 1100 cm⁻¹ and 1200 cm⁻¹ (in particular feature h) suggest that the lowest energy isomer (*trans*-1) is indeed the isomer populated in the experiment.

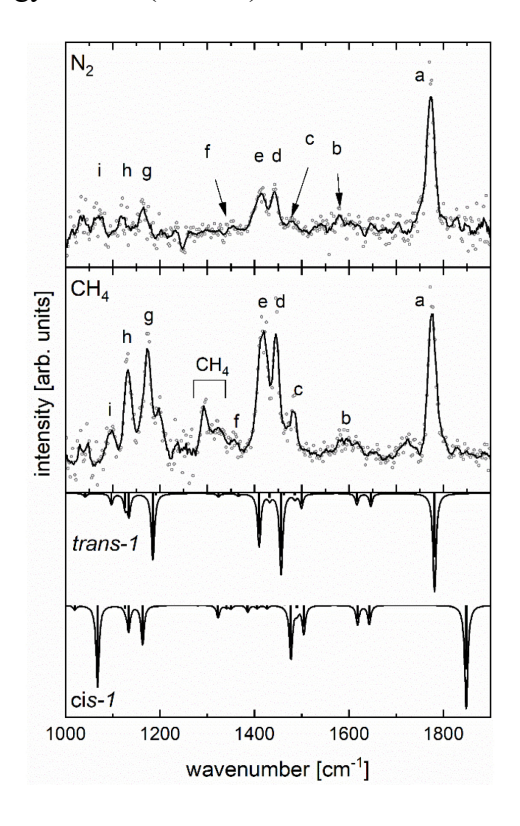


Figure 3. IR photodissociation spectra (upright) of ValH⁺·N₂ (top) and ValH⁺·CH₄ (second from top) compared to the calculated spectra of different structures of ValH⁺ (inverted, shown on the same vertical scale). The open circles in the experimental spectra are raw data points, the full lines are 5-point gliding averages to guide the eye. The tag is given for each experimental spectrum, and the structure label is shown for each calculated spectrum (see Figure 2). See text for letter labels in the experimental spectra. Vertical bars mark individual calculated transitions.

Tags generally bind to an ion in the vicinity of the charge center, and usually have only small effects on the structure and spectrum. Consistent with this expectation, exploratory calculations show that the tags bind close to the NH₃⁺ group. Table 1 summarizes the frequency positions of each feature for the two tags used here. For the lowest energy conformation of the tags, there is no significant change in the structure of the ValH⁺ ion (see Supporting Information, Figures S3 and S4), and only small changes in its calculated IR frequencies (Table 1). The experimental values for N₂ and CH₄ deviate somewhat more strongly from each other than the calculations would suggest, but still are within 11 cm⁻¹ for the five most prominent transitions.

Table 1. Experimental (Calculated^a in Parentheses) Frequencies in cm⁻¹ for *trans*-ValH⁺ With Different Tags.

- 4 4		
Label ^b	$\mathrm{CH_4}$	N_2
a	1776 (1782)	1773 (1783)
b	1593 (1636) ^c	1580 (1643) ^c
c	1482 (1499)	1478 (1500)
d	1445 (1464)	1442 (1472)
e	1417 (1411)	1411 (1412)
f	1356 (1367)	1355 (1367)
g	1173 (1184)	1164 (1184)
h	1131 (1133) ^c	1120 (1134) ^c
i	1097 (1104)	1068 (1111)

^a B3LYP functional and cc-pVTZ basis, frequencies scaled by 0.9889.²⁹

^b See Figure 3.

^c Average of two calculated frequencies contributing to this feature.

However, an overall absence of tagging effects on the spectrum cannot be taken for granted. A conformation with an N₂ tag binding in a slightly different position, 59 meV higher in energy (see Supporting Information, Figure S4), is predicted to result in a blue shift of the OCO stretching feature by 10 cm⁻¹, and even an altered intensity pattern in the NH₃⁺ umbrella region. This structure is higher in energy because the tag interferes with the intramolecular H-bond, destabilizing the complex. Since the overall experimental band pattern in the NH₃⁺ umbrella region matches the calculated patterns of the untagged *trans* structures, we judge that this tag position is not significantly populated.

The vibrational signatures of the CH₄ tag itself are found at 1293 cm⁻¹ and 1324 cm⁻¹, respectively, and they represent different CH₃ umbrella modes of the tag. The N₂ stretching frequency is calculated to be at 2431 cm⁻¹, which is outside the frequency range reported here.

A much more dramatic influence of the tag is observed for the relative intensities for the experimental IR spectra. While the relative intensities in the spectrum of ValH⁺·CH₄ are consistent with the calculated pattern, the intensities for ValH⁺·N₂ show a pronounced dependence on frequency, with the lower frequency modes having significantly lower relative intensities than calculated. We trace this behavior to the tag binding energies. The binding energy of the N₂ tag is calculated to be significantly higher than the CH₄ tag (see Table 2), with binding energies of the former in the range of the photon energies in the present work, while the latter was calculated on average 500 cm⁻¹ lower than for N₂, closer to the low energy end of the spectral range discussed here.

Table 2. Calculated Binding Energies in cm⁻¹ for ValH⁺ in Complexes with Different Tags.

Method	CH ₄	N_2
B3LYP/cc-pVTZ	1008	1400
CCSD/cc-pVDZ	900	1586
CCSD/cc-pVTZ	1257	1498
CCSD(T)/cc-pVDZ	973	1670

Tagged ValH⁺ ions spend roughly 20 μ s between photon absorption and entry into the reflectron. If they require significantly longer times for dissociation, our experiment will not register fragment ion formation. To evaluate the effect of the binding energy E_0 on the photodissociation efficiency, we estimated the energy-dependent rate constants k(E) for unimolecular dissociation of photoexcited ValH⁺·N₂ and ValH⁺·CH₄ complexes based on Rice-Ramsperger-Kassel-Marcus (RRKM) theory⁵¹⁻⁵⁴ as

$$k(E) = \frac{sN^{\ddagger}(E - E_0)}{h\rho(E)},$$

where E is the total internal energy of the complex, s is the reaction degeneracy (here taken to be 1), $N^{\ddagger}(E)$ is the sum of vibrational states at the transition state, h is Planck's constant, and $\rho(E)$ is the vibrational density of states of the reactant complex. Since we cannot measure actual dissociation rate constants, we chose several approximations to simplify the calculation of the sum and density of states for estimated values of k(E): (i) all vibrational modes are treated as harmonic oscillators; (ii) we assume a tight transition state by identifying a single vibration of the reactant complex (calculated at 106 cm^{-1}) as a reaction coordinate that most closely resembles dissociation of the complex; (iii) the methyl groups are treated as hindered rotors in a 3-fold well to better

represent their degeneracy (g = 3), but the level spacing was still chosen to be harmonic; (iv) similar to (iii), the internal rotations of the N₂ tag were treated as hindered rotors in a double well, resulting in a degeneracy g = 2. These simplifications allowed us to estimate the sums and densities of states using a simple Beyer-Swinehart algorithm.⁵⁵

In addition to the energy of the absorbed photon, the ions have an internal energy based on their microcanonical temperature prior to photon absorption. In previous work, ⁵⁶ we estimated that the ions prepared at ca. 30 K trap temperature will have microcanonical temperatures of ca. 65 K. The internal energy of the tagged ion is given by

$$U_{vib} = \sum_{j} \frac{\hbar \omega_{j}}{e^{\frac{\hbar \omega_{j}}{k_{B}T}} - 1},$$

where the sum runs over all vibrational frequencies, resulting in internal energies of 150 cm⁻¹ for N₂-tagged ions, which we simply add to the photon energy $\hbar\omega$ to arrive at the total energy after photon absorption. For CH₄-tagged ions, the higher temperature of the trap increases the estimated ion temperature to 95 K, which results in internal energies of ca. 365 cm⁻¹ prior to photon absorption. If the total energy $(U_{vib} + \hbar\omega)$ is below the calculated dissociation energy E_0 , we expect no dissociation to occur. Above this threshold, the characteristic time scales for dissociation depend on the photon energy and can still be longer than the experimental observation time of 20 μ s in our setup. For ValH⁺·N₂, significant suppression of the photodissociation quantum yield can be expected for photon energies as high as 1735 cm⁻¹ (see Figure 4 and Supporting Information, Figure S5) based on the calculated binding energies shown in Table 2. In the spectrum of ValH⁺·N₂, feature (b) at 1580 cm⁻¹ is significantly suppressed compared to the same feature in the spectrum of ValH⁺·CH₄ (Figure 3), consistent with a binding energy of the N₂ tag around 1600 cm⁻¹ or higher. The lack of any apparent suppression of signals for the CH₄ tag in the spectral range

considered here is consistent with significantly lower binding energies (see Table 2, Figure 4, and Supporting Information, Figure S5) as well as higher internal energy contents of the tagged ion due to the higher trap temperature.

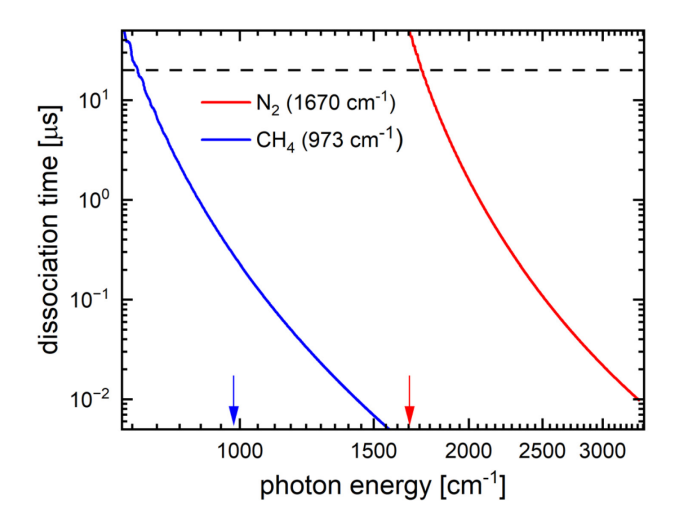


Figure 4. IR photodissociation times of ValH⁺·N₂ (red trace) and ValH⁺·CH₄ (blue trace) based on RRKM calculations and dissociation energies from CCSD(T) calculations (see Table 2). Both axes are logarithmic. The tag dissociation energies are indicated by vertical arrows. The horizontal dashed line shows the detection time window, i.e., dissociation times above this line will lead to suppressed photodissociation efficiency.

Based on the calculated binding energies and the RRKM estimates, we judge that N₂ binds sufficiently strongly to the ion to suppress the photodissociation quantum yield at photon energies significantly below the feature of the antisymmetric OCO stretching vibration. The residual fragment ion yield at low photon energies is likely caused by a fraction of the ion population that are incompletely thermalized, or which are collisionally excited below the threshold for dissociation during ejection from the ion trap. In contrast, tagging with CH₄ does not lead to suppression of the photodissociation quantum yield in the fingerprint region. We note that – although this is not the subject of the present work – tagging with D₂ seems to have not led to

significant suppression of the photodissociation quantum yield in work on other protonated amino acids by Garand and coworkers down to 1400 cm⁻¹.

Coming back to the motivation for this work, the choice of the best tag will depend on several factors. The photodissociation quantum yield of the tag in the relevant frequency range is of obvious importance for the signal-to-noise ratio and the faithful representation of the IR absorption spectrum in the photodissociation channel. Out of the currently known tags for protonated amino acids, this consideration favors the use of D₂ or CH₄, although there should be no problems associated with N₂ tags for work in the CH and OH stretching regions (above ca. 2700 cm⁻¹). Even water as a "tag", which can be used at trap temperatures in the range of 80 - 185 K, which can be used at trap temperatures in the range of 80 - 185 K, and work in this spectral region, 12, 14, 57 although the presence of a water adduct may change the spectrum of the biomarker considerably. Complexes of protonated amino acids with water adducts formed in an ESI source at room temperature can be dissociated by IRMPD even in the fingerprint region.¹⁸, ⁵⁷ For an instrument on a planetary probe, a very important consideration is the temperature of the target environment. Since heating and cooling can be energy and weight intensive, the optimal tagging temperature should be as close to the target environment as possible. This excludes D₂, and even N₂ will be impractical to use on most target worlds (see Introduction). Depending on the exact region on a world like Europa or Enceladus, CH₄ shows the most promise of the tags studied so far, although Ceres and Titan will likely be too warm. It would be advantageous to study additional tags, such as CF₄ or CH₃CN, for their potential use at higher temperatures.

Conclusions

We have used CIVS to measure the IR fingerprint spectra of protonated Val (ValH⁺), comparing the experimental spectra of ValH⁺ tagged with N₂ and CH₄. Based on the calculated spectra of potential conformers, we find that the *trans* conformer dominates the population, consistent with the fact that it is calculated to be lowest in energy. The different tags have only a small influence on most of the vibrational energies, but N₂ has a much higher binding energy than CH₄. As a result, the photodissociation efficiency for ValH⁺·N₂ is strongly suppressed for all but the highest energy feature in the spectrum at 1773 cm⁻¹, consistent with simple RRKM calculations. Interestingly, this observation may make N₂ a more generally unattractive tag for CIVS of protonated amino acids in the lower energy part of the fingerprint region. In contrast, CH₄, which can be used at higher trap temperatures (we found 60 K to be optimal) without introducing significant broadening, making it a suitable tag for applications of CIVS with protonated amino acids, particularly in experiments that require trap temperatures above 50 K. For example, the use of CH₄ tags would allow application of messenger tagging on planetary missions to target worlds such as Europa or Enceladus.

ASSOCIATED CONTENT

Supporting Information. The following files are available free of charge: Calculated IR spectra of protonated valine and selected isomers; calculated IR spectra and lowest energy structures of *trans*-ValH⁺; lowest energy structures of ValH⁺, ValH⁺·N₂ and ValH⁺·CH₄; calculated IR spectra and lowest energy structures of ValH⁺·N₂; IR photodissociation times of ValH⁺·N₂ and ValH⁺·CH₄; atomic coordinates for ValH⁺, ValH⁺·N₂, and ValH⁺·CH₄; unscaled vibrational frequencies of ValH⁺·N₂ and ValH⁺·CH₄.

AUTHOR INFORMATION

Corresponding Author

*J. Mathias Weber – JILA and Department of Chemistry, University of Colorado, Boulder,

Colorado 80309-0440, United States; orcid.org/0000-0002-5493-5886; Phone: +1-303-492-7841;

Email: weberjm@jila.colorado.edu

Notes

The authors declare no competing financial interest.

ACKNOWLEDGMENT

This work is published in remembrance of our co-author and colleague Dr. Frank Maiwald.

Portions of this work were funded by the Jet Propulsion Laboratory, California Institute of

Technology, under a contract with the National Aeronautics and Space Administration

(80NM0018D0004) and JPL's Strategic University Research Partnership (SURP) program. We

gratefully acknowledge partial support from the National Science Foundation under award no.

CHE-2154271. This work utilized resources from the University of Colorado Boulder Research

Computing Group, which is supported by the National Science Foundation (awards ACI-1532235

and ACI-1532236), the University of Colorado Boulder, and Colorado State University.

19

REFERENCES

- (1) McGuire, B. A. 2021 Census of Interstellar, Circumstellar, Extragalactic, Protoplanetary Disk, and Exoplanetary Molecules. *Astrophys. J. Suppl. Ser.* **2022**, *259*, 30.
- (2) Fujii, Y.; Angerhausen, D.; Deitrick, R.; Domagal-Goldman, S.; Grenfell, J. L.; Hori, Y.; Kane, S. R.; Pallé, E.; Rauer, H.; Siegler, N.; et al. Exoplanet Biosignatures: Observational Prospects. *Astrobiology* **2018**, *18*, 739-778.
- (3) Brockwell, T. G.; Waite, J. H.; Lunine, J. I.; Meech, K. J.; Miller, G.; Wilson, P.; Pickens, K.; Roberts, J.; Ieee. The MAss Spectrometer for Planetary Exploration (MASPEX). In *IEEE Aerospace Conference*, Big Sky, MT, Mar 05-12, 2016; IEEE 2016.
- (4) Willis, P.; Mora, M. F.; Noell, A.; Creamer, J.; Kehl, F.; Zamuruyev, K.; Jaramillo, E.; Kok, M.; Cieslarova, Z.; Santos, M. S. F.; et al. How to Search for Chemical Biosignatures on Ocean Worlds. *Bull. Am. Astronom. Soc.* **2020**, *53*, Whitepaper 293.
- (5) Chou, L. T.; Mahaffy, P.; Trainer, M.; Eigenbrode, J.; Arevalo, R.; Brinckerhoff, W.; Getty, S.; Grefenstette, N.; Da Poian, V.; Fricke, G. M.; et al. Planetary Mass Spectrometry for Agnostic Life Detection in the Solar System. *Front. Astron. Space Sci.* **2021**, 8.
- (6) Linstrom, P. J.; Mallard, W. G. NIST Chemistry WebBook, NIST Standard Reference Database Number 69. National Institute of Standards and Technology: Gaithersburg MD, 20899, retrieved September 12, 2023.
- (7) Schäfer, A.; Debnath, S.; Tränkle, J.; Mohr, T.; Kappes, M. M. Acriflavine Is More than It Seems: Resolving Optical Properties of Multiple Isomeric Constituents at 5 K. *J. Phys. Chem. Lett.* **2024**, 7295-7301.

- (8) Kapota, C.; Lemaire, J.; Maitre, P.; Ohanessian, G. Vibrational signature of charge solvation vs salt bridge isomers of sodiated amino acids in the gas phase. *J. Am. Chem. Soc.* **2004**, *126*, 1836-1842.
- (9) Polfer, N. C.; Paizs, B.; Snoek, L. C.; Compagnon, I.; Suhai, S.; Meijer, G.; von Helden, G.; Oomens, J. Infrared Fingerprint Spectroscopy and Theoretical Studies of Potassium Ion Tagged Amino Acids and Peptides in the Gas Phase. *J. Am. Chem. Soc.* **2005**, *127*, 8571-8579.
- (10) Mac Aleese, L.; Simon, A.; McMahon, T. B.; Ortega, J. M.; Scuderi, D.; Lemaire, J.; Maitre, P. Mid-IR spectroscopy of protonated leucine methyl ester performed with an FTICR or a Paul type ion-trap. *Int. J. Mas Spectrom.* **2006**, *249*, 14-20.
- (11) Oomens, J.; Sartakov, B. G.; Meijer, G.; Von Helden, G. Gas-phase infrared multiple photon dissociation spectroscopy of mass-selected molecular ions. *Int. J. Mas Spectrom.* **2006**, *254*, 1-19.
- (12) Kamariotis, A.; Boyarkin, O. V.; Mercier, S. R.; Beck, R. D.; Bush, M. F.; Williams, E. R.; Rizzo, T. R. Infrared spectroscopy of hydrated amino acids in the gas phase: Protonated and lithiated valine. *J. Am. Chem. Soc.* **2006**, *128*, 905-916.
- (13) Vaden, T. D.; de Boer, T. S. J. A.; MacLeod, N. A.; Marzluff, E. M.; Simons, J. P.; Snoek, L. C. Infrared spectroscopy and structure of photochemically protonated biomolecules in the gas phase: a noradrenaline analogue, lysine and alanyl alanine. *Phys. Chem. Chem. Phys* **2007**, *9*, 2549-2555.
- (14) Bush, M. F.; Prell, J. S.; Saykally, R. J.; Williams, E. R. One Water Molecule Stabilizes the Cationized Arginine Zwitterion. *J. Am. Chem. Soc.* **2007**, *129*, 13544-13553.

- (15) Stearns, J. A.; Mercier, S.; Seaiby, C.; Guidi, M.; Boyarkin, O. V.; Rizzo, T. R. Conformation-specific Spectroscopy and photodissociation of cold, protonated tyrosine and phenylalanine. *J. Am. Chem. Soc.* **2007**, *129*, 11814-11820.
- (16) Forbes, M. W.; Bush, M. F.; Polfer, N. C.; Oomens, J.; Dunbar, R. C.; Williams, E. R.; Jockusch, R. A. Infrared spectroscopy of arginine cation complexes: Direct observation of gasphase zwitterions. *J. Phys. Chem. A* **2007**, *111*, 11759-11770.
- (17) Correia, C. F.; Balaj, P. O.; Scuderi, D.; Maitre, P.; Ohanessian, G. Vibrational signatures of protonated, phosphorylated amino acids in the gas phase. *J. Am. Chem. Soc.* **2008**, *130*, 3359-3370.
- (18) Wu, R. H.; McMahon, T. B. An Investigation of Protonation Sites and Conformations of Protonated Amino Acids by IRMPD Spectroscopy. *ChemPhysChem* **2008**, *9*, 2826-2835.
- (19) O'Brien, J. T.; Prell, J. S.; Steill, J. D.; Oomens, J.; Williams, E. R. Interactions of Monoand Divalent Metal Ions with Aspartic and Glutamic Acid Investigated with IR Photodissociation Spectroscopy and Theory. *J. Phys. Chem. A* **2008**, *112*, 10823-10830.
- (20) Polfer, N. C.; Oomens, J. Vibrational Spectroscopy of Bare and Solvated Ionic Complexes of Biological Relevance. *Mass Spectrom. Rev.* **2009**, *28*, 468-494.
- (21) Heaton, A. L.; Bowman, V. N.; Oomens, J.; Steill, J. D.; Armentrout, P. B. Infrared Multiple Photon Dissociation Spectroscopy of Cationized Asparagine: Effects of Metal Cation Size on Gas-Phase Conformation. *J. Phys. Chem. A* **2009**, *113*, 5519-5530.
- (22) Rizzo, T. R.; Stearns, J. A.; Boyarkin, O. V. Spectroscopic studies of cold, gas-phase biomolecular ions. *Int. Rev. Phys. Chem.* **2009**, *28*, 481-515.

- (23) Oomens, J.; Steill, J. D.; Redlich, B. Gas-Phase IR Spectroscopy of Deprotonated Amino Acids. *J. Am. Chem. Soc.* **2009**, *131*, 4310-4319.
- (24) Citir, M.; Stennett, E. M. S.; Oomens, J.; Steill, J. D.; Rodgers, M. T.; Armentrout, P. B. Infrared multiple photon dissociation spectroscopy of cationized cysteine: Effects of metal cation size on gas-phase conformation. *Int. J. Mas Spectrom.* **2010**, *297*, 9-17.
- (25) Brodbelt, J. S. Photodissociation mass spectrometry: new tools for characterization of biological molecules. *Chem. Soc. Rev.* **2014**, *43*, 2757-2783.
- (26) Patrick, A. L.; Polfer, N. C. Peptide Fragmentation Products in Mass Spectrometry Probed by Infrared Spectroscopy. In *Gas-Phase IR Spectroscopy and Structure of Biological Molecules*, Rijs, A. M., Oomens, J. Eds.; Topics in Current Chemistry-Series, Springer Cham, 2015; pp 153-181.
- (27) Rijs, A. M.; Oomens, J. IR Spectroscopic Techniques to Study Isolated Biomolecules. In *Gas-Phase IR Spectroscopy and Structure of Biological Molecules*, Rijs, A. M., Oomens, J. Eds.; Topics in Current Chemistry-Series, Springer Cham, 2015; pp 1-42.
- (28) Voss, J. M.; Fischer, K. C.; Garand, E. Accessing the Vibrational Signatures of Amino Acid Ions Embedded in Water Clusters. *J. Phys. Chem. Lett.* **2018**, *9*, 2246-2250.
- (29) Fischer, K. C.; Sherman, S. L.; Voss, J. M.; Zhou, J.; Garand, E. Microsolvation Structures of Protonated Glycine and L-Alanine. *J. Phys. Chem. A* **2019**, *123*, 3355-3366.
 - (30) Ashkenazy, Y. The surface temperature of Europa. Heliyon 2019, 5, e01908.

- (31) Spencer, J. R.; Pearl, J. C.; Segura, M.; Flasar, F. M.; Mamoutkine, A.; Romani, P.; Buratti, B. J.; Hendrix, A. R.; Spilker, L. J.; Lopes, R. M. C. Cassini Encounters Enceladus: Background and the Discovery of a South Polar Hot Spot. *Science* **2006**, *311*, 1401-1405.
- (32) Tosi, F.; Capria, M. T.; De Sanctis, M. C.; Ammannito, E.; Capaccioni, F.; Zambon, F.; Raponi, A.; Russell, C. T.; Raymond, C. A. Dwarf Planet Ceres: Preliminary Surface Temperatures from Dawn. In *Geophysical Research Abstracts*, EGU General Assembly, Vienna, Austria, 2015; p 11960.
- (33) Jennings, D. E.; Cottini, V.; Nixon, C. A.; Achterberg, R. K.; Flasar, F. M.; Kunde, V. G.; Romani, P. N.; Samuelson, R. E.; Mamoutkine, A.; Gorius, N. J. P.; et al. Surface Temperatures on Titan During Northern Winter and Spring. *Astrophys. J. Lett.* **2016**, *816*, L17.
- (34) Asvany, O.; P, P. K.; Redlich, B.; Hegemann, I.; Schlemmer, S.; Marx, D. Understanding the Infrared Spectrum of Bare CH₅⁺. *Science* **2005**, *309*, 1219-1222.
- (35) Chakrabarty, S.; Holz, M.; Campbell, E. K.; Banerjee, A.; Gerlich, D.; Maier, J. P. A Novel Method to Measure Electronic Spectra of Cold Molecular Ions. *J. Phys. Chem. Lett.* **2013**, *4*, 4051-4054.
- (36) Schmid, P. C.; Asvany, O.; Salomon, T.; Thorwirth, S.; Schlemmer, S. Leak-Out Spectroscopy, A Universal Method of Action Spectroscopy in Cold Ion Traps. *J. Phys. Chem. A* **2022**, *126*, 8111-8117.
- (37) Xu, S.; Gozem, S.; Krylov, A. I.; Christopher, C. R.; Mathias Weber, J. Ligand influence on the electronic spectra of monocationic copper-bipyridine complexes. *Phys. Chem. Chem. Phys.* **2015**, *17*, 31938-31946.

- (38) Chu, P. M.; Guenther, F. R.; Rhoderick, G. C.; Lafferty, W. J. Quantitative Infrared Database. In *NIST Chemistry WebBook, NIST Standard Reference Database Number 69*; Mallard, P. J. L. a. W. G., Ed.; National Institute of Standards and Technology.
- (39) Parr, R. G.; Yang, W. Density-Functional Theory of Atoms and Molecules; Oxford University Press, 1989.
- (40) Becke, A. D. Density-Functional Exchange-Energy Approximation with Correct Asymptotic-Behavior. *Phys. Rev. A* **1988**, *38*, 3098-3100.
- (41) Lee, C. T.; Yang, W. T.; Parr, R. G. Development of the Colle-Salvetti Correlation-Energy Formula into a Functional of the Electron-Density. *Phys. Rev. B* **1988**, *37*, 785-789.
- (42) Dunning, T. H. Gaussian-Basis Sets for Use in Correlated Molecular Calculations .1. the Atoms Boron through Neon and Hydrogen. *J. Chem. Phys.* **1989**, *90*, 1007-1023.
- (43) Woon, D. E.; Dunning, T. H. Gaussian-Basis Sets for Use in Correlated Molecular Calculations .3. the Atoms Aluminum through Argon. *J. Chem. Phys.* **1993**, *98*, 1358-1371.
- (44) Boys, S. F.; Bernardi, F. Calculation of Small Molecular Interactions by Differences of Separate Total Energies Some Procedures with Reduced Errors. *Mol. Phys.* **1970**, *19*, 553-566.
- (45) Simon, S.; Duran, M.; Dannenberg, J. J. How does basis set superposition error change the potential surfaces for hydrogen-bonded dimers? *J. Chem. Phys.* **1996**, *105*, 11024-11031.
- (46) Purvis, G. D., III; Bartlett, R. J. A full coupled-cluster singles and doubles model: The inclusion of disconnected triples. *J. Chem. Phys.* **1982**, *76*, 1910-1918.

- (47) Raghavachari, K.; Trucks, G. W.; Pople, J. A.; Head-Gordon, M. A fifth-order perturbation comparison of electron correlation theories. *Chem. Phys. Lett.* **1989**, *157*, 479-483.
- (48) Bartlett, R. J.; Watts, J. D.; Kucharski, S. A.; Noga, J. Non-iterative fifth-order triple and quadruple excitation energy corrections in correlated methods. *Chem. Phys. Lett.* **1990**, *165*, 513-522.
- (49) Frisch, M. J.; Trucks, G. W.; Schlegel, H. B.; Scuseria, G. E.; Robb, M. A.; Cheeseman, J. R.; Scalmani, G.; Barone, V.; Petersson, G. A.; Nakatsuji, H. et al. *Gaussian 16 Rev. C.01*, Wallingford, CT, 2016.
- (50) Quesada-Moreno, M. M.; Avilés-Moreno, J. R.; López-González, J. J. Structural behavior of neutral, protonated, and deprotonated L-valine in aqueous solutions: a combined study using chirality sensitive (VCD) and non sensitive (IR and Raman) vibrational spectroscopies and quantum chemical calculations. *Tetrahedron: Asymmetry* **2015**, *26*, 1314-1327.
- (51) Rice, O. K.; Ramsperger, H. C. Theories of Unimolecular Gas Reactions at Low Pressures. J. Am. Chem. Soc. 1927, 49, 1617-1629.
 - (52) Kassel, L. S. Studies in Homogeneous Gas Reactions. I. J. Phys. Chem. 1928, 32, 225-242.
- (53) Marcus, R. A. Unimolecular Dissociations and Free Radical Recombination Reactions. *J. Chem. Phys.* **1952**, *20*, 359-364.
- (54) Marcus, R. A.; Rice, O. K. The Kinetics of the Recombination of Methyl Radicals and Iodine Atoms. *J. Phys. Colloid Chem.* **1951**, *55*, 894-908.
- (55) Beyer, T.; Swinehart, D. F. Algorithm 448: number of multiply-restricted partitions. *Commun. ACM* **1973**, *16*, 379.

- (56) Dodson, L. G.; Zagorec-Marks, W.; Xu, S.; Smith, J. E. T.; Weber, J. M. Intrinsic photophysics of nitrophenolate ions studied by cryogenic ion spectroscopy. *Phys. Chem. Chem. Phys* **2018**, *20*, 28535-28543.
- (57) Nguyen, T. M.; Ober, D. C.; Balaji, A.; Maiwald, F. W.; Hodyss, R. P.; Madzunkov, S. M.; Okumura, M.; Nemchick, D. J. Infrared Photodissociation Spectroscopy of Water-Tagged Ions with a Widely Tunable Quantum Cascade Laser for Planetary Science Applications. *Anal. Chem.* **2024**, *96*, 8875–8879.

TOC Graphic

